

Supplementary Information

Nanotherapeutics using all-natural materials. Effective treatment of wound biofilm infections using crosslinked nanoemulsions

Cheng-Hsuan Li^{‡a}, Ryan F. Landis^{‡a}, Jessa Marie Makabenta^{‡a}, Ahmed Nabawy^a, Tiphaine Tronchet^a, Danielle Archambault^b, Yuanchang Liu^a, Rui Huang^a, Morgane Golan^b, Wei Cui^b, Jesse Mager^b, Akash Gupta^a, Suzannah Schmidt-Malan^c, Robin Patel^c, and Vincent M. Rotello^{*a}

^aDepartment of Chemistry, University of Massachusetts Amherst, 710 North Pleasant Street, Amherst, Massachusetts 01003, United States

^bDepartment of Veterinary and Animal Sciences, University of Massachusetts Amherst, 661 North Pleasant Street, Amherst, Massachusetts 01003, United States

^cDivision of Clinical Microbiology, Department of Laboratory Medicine and Pathology, Mayo Clinic, 200 First Street SW, Rochester, MN 55905

[‡]C.-H.L., R.F.L., and J.M.M. contributed equally

Corresponding Author

*E-mail: rotello@chem.umass.edu

Table of contents

Experimental Methods.....	3
Supplementary Table S1 MBICs and MBECs of gelatin nanoemulsions against bacterial biofilms	11
Supplementary Table S2 Information of Bacterial strains from Cooley Dickinson Hospital provided by Dr. Riley	20
Supplementary Table S3 Information of bacterial strains from Mayo Clinic	22
Supplementary Fig S1 Stability and biodegradation of gelatin nanoemulsion.....	8
Supplementary Fig S2 Additional transmission electron microscopy images of the gelatin nanoemulsions.....	8
Supplementary Fig S3 IR spectra of nanoemulsion cross-linking and control experiments	9
Supplementary Fig S4 Killing mechanism of gelatin nanoemulsions.....	10
Supplementary Fig S5 Purulence scoring system	12
Supplementary Fig S6 Colony counts from the infected wounds treated with PBS and vancomycin	13
Supplementary Fig S7 Photographs of infected wounds treated with gelatin nanoemulsions	14
Supplementary Fig S8 Photographs of infected wounds treated with PBS.....	15
Supplementary Fig S9 Photographs of infected wounds treated with vancomycin	16
Supplementary Fig S10 Purulence scores of wounds treated with nanoemulsions, PBS, and vancomycin	17
Supplementary Fig S11 Additional histological samples of skin surrounding infected wounds	18
Supplementary Fig S12 Excised skin after histological sample preparation – macroscopic and microscopic images.	19

Experimental Methods

Materials: Riboflavin, carvacrol, and Nile red were purchased from Acros. Gelatin (Type B, 100 Bloom) and Luria-Burtani (LB) liquid medium were purchased from Fisher Chemical. Phosphate-buffered saline was purchased from HyClone. Sodium chloride and Pepton were purchased from Fisher BioReagents. M9 minimum medium was purchased from Teknova. Tryptic soy broth (TSB) was purchased from Becton Dickinson. AlamarBlue™ cell viability reagent was purchased from Invitrogen. Fetal bovine serum (FBS) was purchased from Gibco. Pegged lids were purchased from Nunc. Paraformaldehyde (PFA) was purchased from Sigma-Aldrich.

Preparation of gelatin nanoemulsions: Nanoemulsions were prepared through emulsification of a suspension of riboflavin in carvacrol into an aqueous gelatin solution, followed by irradiation with 365 nm UV-light. Briefly, suspension of riboflavin in carvacrol (3 μ L, 0.1 wt%) was added to the gelatin aqueous solution (497 μ L, 0.24 mg/ml). This solution was then emulsified for 50 seconds using an amalgamator. The emulsion was then exposed to UV lamp for 20 minutes. The concentration of this nanosemulsion stock solution was defined as 100 v/v% (39 mM of carvacrol)

Characterization: The hydrodynamic diameter of nanoemulsions was measured in triplicate using DLS (Malvern Zetasizer). TEM samples were prepared on 300 square mesh nickel grids with Formvar film (Electron Microscopy Sciences). IR was performed on a Bruker Alpha FTIR spectrophotometer fitted with a platinum ATR QuickSnap sampling module.

Biofilm penetration study: Red fluorescent nanoemulsions were prepared as above, using a solution of Nile red in carvacrol (1 mg/ 1000 μ l). GFP-expressing *K. pneumoniae* biofilms were prepared using the preparation method described below for mono-species biofilms. These biofilms were then treated with prepared red fluorescent nanoemulsions (5 v/v%) for 1 hour at room temperature. A Nikon A1 spectral detector confocal with FLIM module was used to monitor penetration profile of the nanoemulsions. A penetration profile study was performed using Nikon A1 resonant scanning confocal with TIRF module. The images were processed using NIS-Elements.

Evaluation of antimicrobial activity in vitro: Frozen (-80 °C) cultures of all bacteria strains used: a.) Clinical isolates *E. coli* (CD-2), MDR *E. coli* (IDRL-10366), *P. aeruginosa* (CD-1006), MDR *P. aeruginosa* (IDRL-11442), *E. cloacae* complex (CD-1412), MRSA (CD-489), MRSA (IDRL-6169); b.) GFP-expressing *K. pneumoniae* (IDRL-11999); and c.) reference strain *P. aeruginosa* (ATCC 27583) were grown aerobically using Luria-Burtani agar. Overnight cultures of bacteria were prepared by transferring isolated colony from the agar plate to culture tubes with sterile LB broth. Bacterial

cultures were then incubated overnight at 37 °C with agitation (275 rpm), until the stationary phase was reached. Bacteria were then collected by centrifugation (7000 rpm, 5 min) and washed thrice with sodium chloride (0.85%). Subsequently, the culture was resuspended in PBS (1 mL) to determine its OD₆₀₀ (SpectraMax M2, Molecular Devices). All clinical isolates with code CD were obtained from Cooley Dickinson Hospital, while those denoted by IDRL were from the Infectious Diseases Research Laboratory in Mayo Clinic.

For mono-species biofilms, bacteria (except *S. aureus*) were prepared by dilution with M9 medium to 0.1 OD₆₀₀ for biofilm formation. For *S. aureus* biofilms, cultures were prepared in M9/TSB (85:15) to the same concentration. Subsequently, the seeding solutions (100 µL) were added to each well of a 96-well clear flat-bottomed plate. The plate was covered and incubated under static conditions at room temperature overnight. The seeding solutions were removed, and biofilms were washed thrice with PBS. Gelatin nanoemulsion solutions ranging from 0 to 48 v/v% were then administered (100 µL) to the biofilms. The plates were incubated statically at 37 °C. After 3 h, the biofilms were washed thrice with PBS; then alamarBlue™ cell viability reagent¹ (10 v/v%) was added to each well, and incubated for 1 h. Biofilm viability was determined by measuring fluorescence intensity (excitation: 560 nm; emission: 590 nm). Readings from the wells containing alamarBlue™ cell viability reagent (10 v/v%) alone were considered as the blank (I_{blank}), and readings from wells with untreated biofilms were used as growth controls ($I_{control}$). Biofilm viability was calculated using the equation below:

$$Biofilm\ viability\ (\%) = 100\% \times \frac{I_{sample} - I_{blank}}{I_{control} - I_{blank}}$$

Biofilm-3T3 fibroblast cell coculture model was performed using the previously reported protocol.² Briefly, NIH 3T3 (ATCC CRL-1658) cells (20k/ well) were cultured in wells of a 96 well plate overnight to form a monolayer. Afterward, the mammalian cells were washed and 100 µL of bacterial seeding solutions (10⁸ CFU/mL) were added. The cocultures were then stored at 37 °C for six hours without shaking. Gelatin nanoemulsions and other control solutions were diluted in DMEM media prior to use to obtain the desired testing concentrations. The cocultures were washed again and the freshly prepared testing solutions were then added. After 3 h incubation at 37 °C, the cocultures were then analyzed using LDH cytotoxicity assay. To determine the bacteria viability in biofilms, the testing solutions were removed and cocultures were washed with PBS. Fresh PBS was then added, and the plate was sealed and sonicated for 20 min to disperse biofilms. The solutions containing dispersed bacteria were quantitatively determined using colony counting forming unit method.

For the SWF experiment, we followed an established SWF protocol.³ Briefly, bacterial cultures were prepared using the method described above. Biofilm seeding solutions were

prepared in SWF/TSB (1:1) solutions. SWF was comprised of fetal bovine serum (50%) and sodium chloride (50%) in Pepton water (0.1%). This seeding solution (100 μ L) was added to each well of the 96-well plate. The plate was covered and incubated under static conditions at \sim 23 $^{\circ}$ C for 4 days. The activity of gelatin nanoemulsions towards this model was determined using quantitative colony counting.

MBIC and MBBC assays⁴ of single- and dual-species biofilms were carried out using a Calgary biofilm device.⁵ For the single-species biofilms, bacteria were grown in TSB (2.5 mL) at 275 rpm and 37 $^{\circ}$ C until the concentration reached 0.5 McFarland standard. These solutions (150 μ L) were then transferred to each well of a 96-well plate. The plate was covered with a pegged lid and incubated for 6 h at 50 rpm and 37 $^{\circ}$ C. The pegged lid was then removed, rinsed with PBS for 30 seconds, and then transferred to a plate with antimicrobial agents (200 μ L) in each well. MBIC values were determined after the plate was incubated 24 h at 37 $^{\circ}$ C statically. Subsequently, the same pegged lid was rinsed with PBS for 30 seconds again, and transferred to a plate with broth (200 μ L) in each well. MBBC values were determined after the plates were statically incubated for another 24 hours at 37 $^{\circ}$ C. For dual-species biofilms, the same procedure was followed except that 75 μ L of each of the component bacterial species were added into the 96-well microplate then mixed.

Study of killing mechanism of gelatin nanoemulsions: Bacteria solution ($OD_{600} = 0.5$) containing propidium iodide (PI) (10 μ L/ 1000 μ L) was prepared for the killing mechanism study. The bacteria solutions (50 μ L) were added to each well of a black 96-well flat-bottomed plate. Fluorescence intensities were measured immediately after adding 50 μ L of PBS containing 0.125 to 4X MIC of gelatin nanoemulsions or Ceftazidime (Excitation/Emission: 535 nm/ 617 nm).

Ethics statement: C57BL/6 mice were supplied by Jackson Laboratory. Mice were housed in sterile cages with a 12 hours light/ 12 hours dark cycle. They were allowed to acclimatize for at least a week before any of the procedures were carried out. All animal experiments were performed in accordance with the authorized protocol (IACUC Protocol ID 2018-0011) and the policies issued by Institutional Animal Care and Use Committee at University of Massachusetts Amherst.

In vivo wound biofilm murine model: The biofilm model was generated using C57BL/6 mice that were anesthetized and the skin on their dorsum shaved and disinfected using a sterile alcohol pad.⁶ Afterwards, a sterile 5-mm circular full thickness skin wound was punched using a skin puncture biopsy tool. Using a micropipette, 10^7 colony forming units (CFU) of a clinical isolate of

MRSA (IDRL-6169) in saline (10 μ L) was inoculated onto the wound bed. Semi-occlusive transparent Tegaderm[®] was placed over the wound using Mastisol[®] as an adhesive to prevent secondary bacterial contamination. Biofilm was then allowed to form for four days. The mice were then separated into three groups of five: one group treated with nanoemulsions (100% v/v; 39 mM), a second with vancomycin (110 mg/kg) that served as the positive control and a third with vehicle control (saline solution only). Test agents (100 μ L) were administered every other day until the day of sacrifice (day 5); nanoemulsions and saline were administered topically, while vancomycin was injected intraperitoneally. Photographs were taken daily, and purulence scores, wound sizes and weights of the mice were monitored every day. On the day of the sacrifice, the mice were euthanized via CO₂ asphyxiation. Then, 10-mm circular full thickness skin covering the infection area was collected using a skin biopsy punch for histological analysis.

In vivo wound closure measurement and purulence score grading: All photographs were taken from a standard height at the same time over the entire treatment period. Three blinded observers determined the sizes of the wounds using the taken images with ImageJ software and graded the degree of pus formation using a standard purulence scoring system. At the same time, a blinded observer present through the duration of the study measured wound size using a digital caliper (Neiko tools) and rated the degree of purulence of the mice.

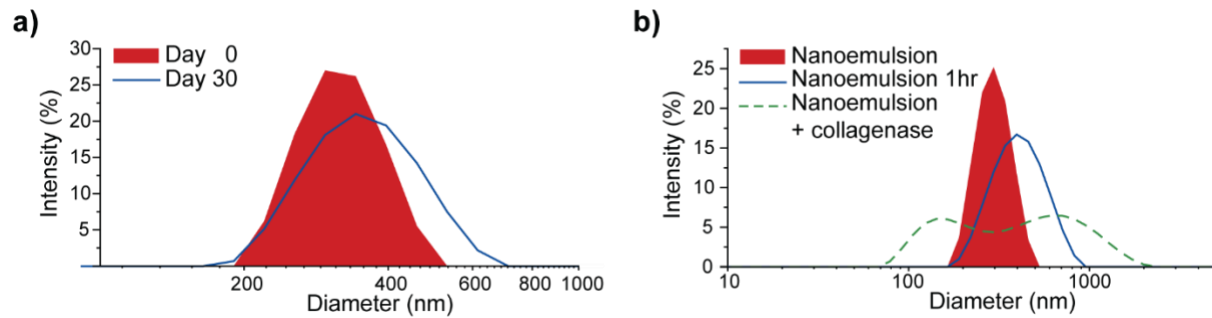
Preparation of skin samples for histological analysis: The skin tissue was fixed in paraformaldehyde (4%) in 4 °C overnight and transferred into PBS. After 24 hours, the tissue was dehydrated in a series of ethanol washes and stored at 4 °C. The tissue samples were cut, dividing the wound in half (Figure S8, Supporting Information). Subsequently, the tissues were cleared in xylene for 1 hour, with a xylene change after 30 minutes. After 1 hour, xylene was removed and replaced with paraffin wax, followed by fresh wax changes every 30 minutes. Half tissue sections were aligned in the wax and sectioned at 7 μ m.

Hematoxylin and eosin (H&E) staining: The sectioned tissues were deparaffinized and rehydrated for subsequent procedures. Slides were then stained with hematoxylin for 45 seconds, placed under gently running tap water for 1 minute, submerged in Scott's Tap Water Substitute (20 g MgSO₄ and 3.5 g NaHCO₂ in 1 L of Milli-Q[®] H₂O) for 1 minute, and then washed in still tap water for another minute. Slides were quickly dipped into ethanol (95%), stained with eosin for 15 seconds, and then again washed in ethanol (95%) with two 2-minute washes in ethanol (100%). Lastly, slides were washed with xylene three times for 1 minute each, and then sealed with

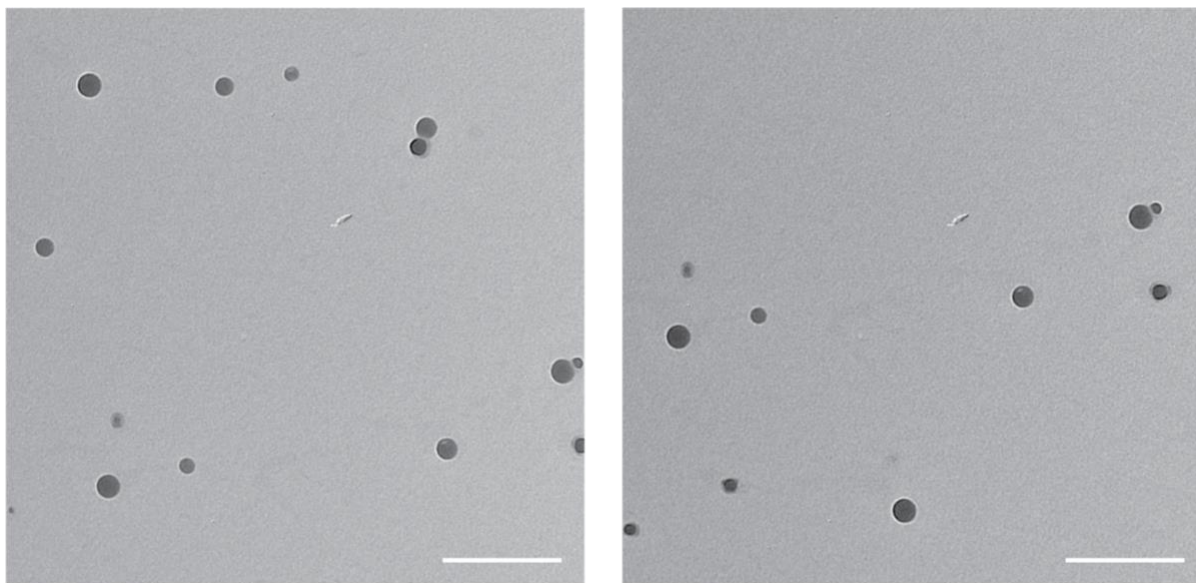
Cytoseal™ 60. H&E stained sections were imaged with a Panoramic MIDI II slide scanner (3DHISTECH).

In vivo antimicrobial activity: Separate experiments were done to assess bacterial reduction midway through the wound healing process. After formation of 4-day old MRSA biofilms on wounds as above, mice were separated into groups of five for each treatment group: nanoemulsions (100% v/v; 39 mM), saline solution only and vancomycin (110 mg/kg). Treatments were administered every other day until the day of sacrifice (day 2). At day 2, mice were sacrificed 3 h after test materials were administered. The mice were euthanized via CO₂ asphyxiation. Then, 3-mm circular full thickness skin in the inner portion of the infection area was collected using a skin biopsy punch for quantitative colony counting. Skin samples were homogenized in PBS, diluted and plated into mannitol salt agar to quantitatively determine remaining bacteria counts.

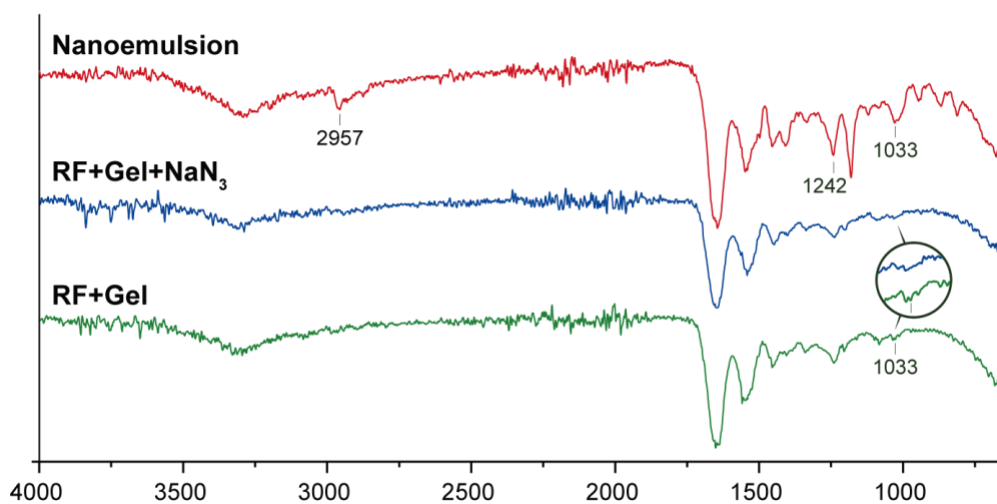
Supplementary Display Items



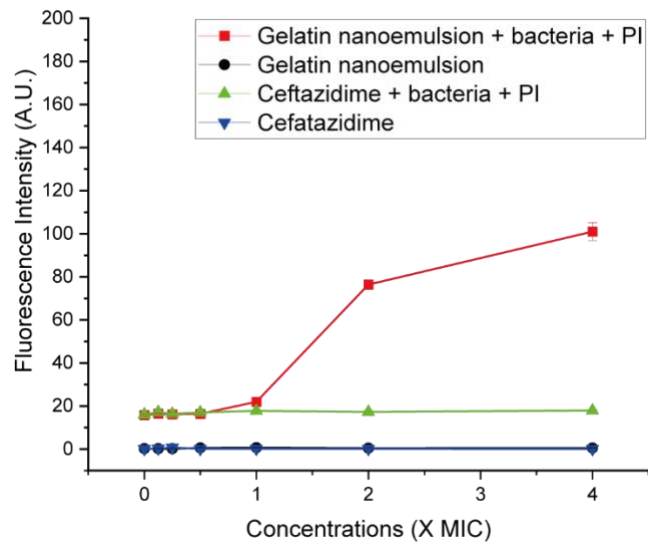
Supplementary Fig S1 | Stability and biodegradation of gelatin nanoemulsion. **a**, Gelatin nanoemulsion demonstrates ≥ 30 days stability at room temperature. Cross-linked nanoemulsions were stable in storage, with only a modest change in DLS. **b**, Collagenase type I degrades the gelatin nanoemulsion at 37°C. The broadened DLS profile indicates the degradation of nanoemulsion.



Supplementary Fig S2 | Additional transmission electron microscopy images of the gelatin nanoemulsions. Scale bar is 500 nm.



Supplementary Fig S3 | IR spectra of nanoemulsion cross-linking and control experiments. As reported previously^{7, 8}, irradiation of riboflavin with UV-A light generates singlet oxygen, oxidizing the imidazole moiety of the histidines of collagen to electrophilic imidazolones. These imidazolones then react with hydroxyl moieties of hydroxyproline, serine, or tyrosine, resulting in cross-linking. Cross-linking after irradiation was demonstrated by the emergence of a band at 1033 cm^{-1} arising from aliphatic-aromatic ether formation, similar to that obtained from riboflavin and gelatin without carvacrol. Compared with irradiation of gelatin and riboflavin alone, carvacrol nanoemulsions featured broadening at 1033 cm^{-1} , an additional aromatic ether signature at 1242 cm^{-1} , and appearance of sp^3 C-H stretches at 2957 cm^{-1} , consistent with an imidazolone reaction with the hydroxyl groups of carvacrol, imparting further hydrophobic domains and additionally stabilizing the oil domains. Irradiation in the presence of the singlet oxygen inhibitor sodium azide resulted in no new bands, consistent with the proposed cross-linking mechanism. All three reactions underwent dialysis and were lyophilized to remove by-product noise (riboflavin, residual carvacrol oil, sodium azide, and water) prior to the IR measurement.



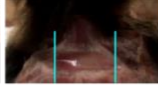
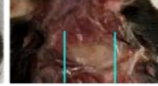
Supplementary Fig S4 | Killing mechanism of gelatin nanoemulsions. *P. aeruginosa* (ATCC-27853) was treated with gelatin nanoemulsions and Ceftazidime in concentrations ranging from 0.125 to 4X of MIC. Upon addition, gelatin nanoemulsions quickly disrupted bacterial cell membrane, therefore allowing propidium iodide to bind to nucleic acids and generate fluorescence. However, no fluorescence was observed with Ceftazidime, as its mechanism of action is through inhibition of enzymes for cell-wall synthesis rather than membrane disruption.

Supplementary Table S1 | MBICs and MBECs of gelatin nanoemulsions against bacterial biofilms

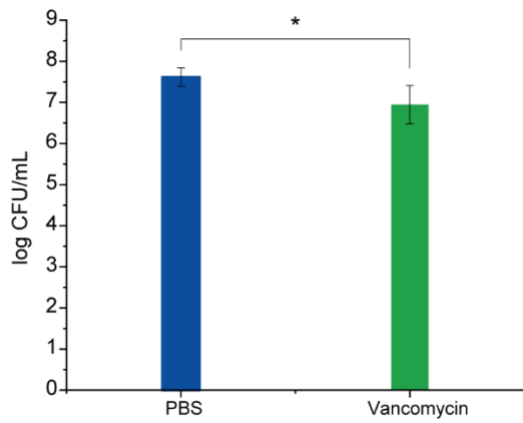
	Single-species biofilms					Dual-species biofilms	
Species	<i>P. aeruginosa</i>			<i>E. coli</i>	<i>S. aureus</i>	<i>S. aureus</i> + <i>P. aeruginosa</i>	<i>S. aureus</i> + <i>E. coli</i>
Strain	CD-1006	IDRL-11442 ²	ATCC 27583	IDRL-10366 ²	IDRL-6169 ¹	IDRL-6169 ¹ + IDRL-11442 ²	IDRL-6169 ¹ + IDRL-10366 ²
MBIC	4%	4%	8%	4%	4%	4%	4%
MBEC	4%	4%	8%	4%	4%	4%	4%

¹Methicillin-resistant

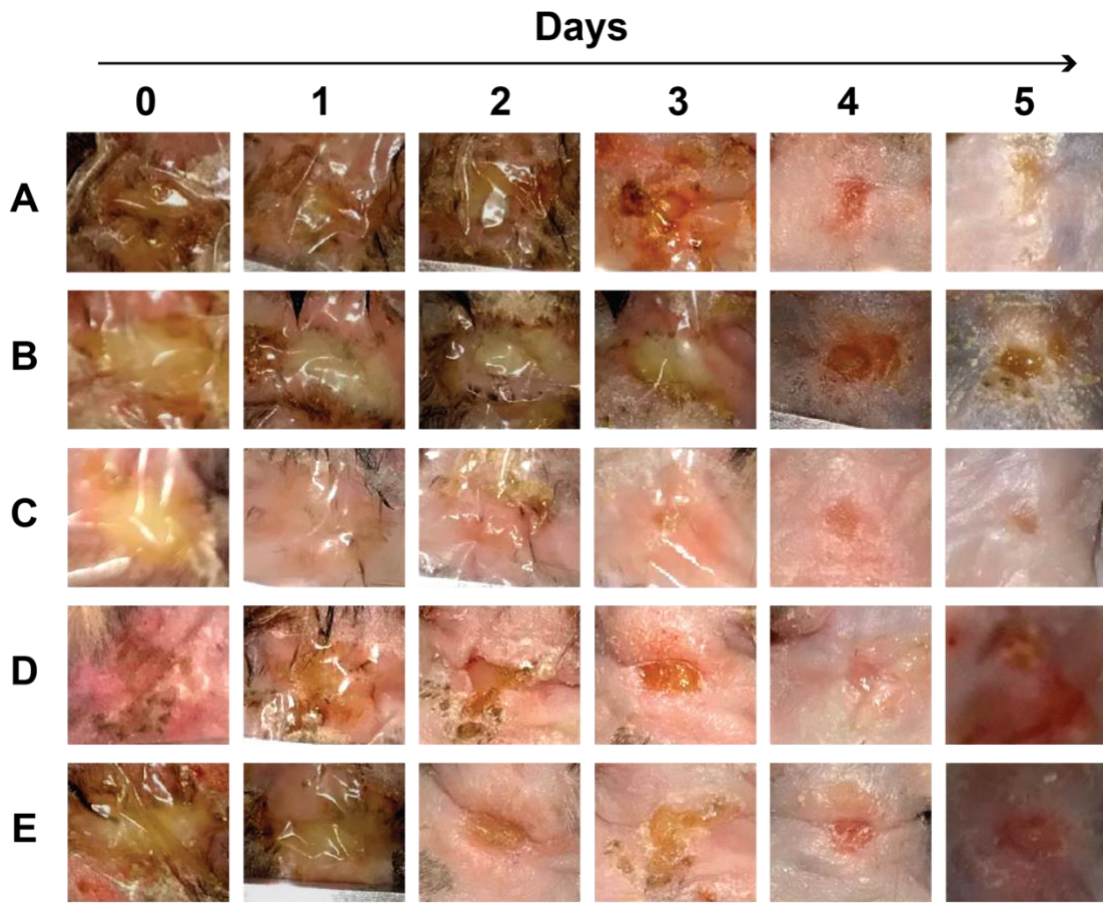
²Multidrug-resistant

Purulence score	0	1	2	3	4	5
Photo						
Description	normal wound bed	slight turbid exudate	mild whitish exudate	whitish exudate	yellowish exudate	gross pus

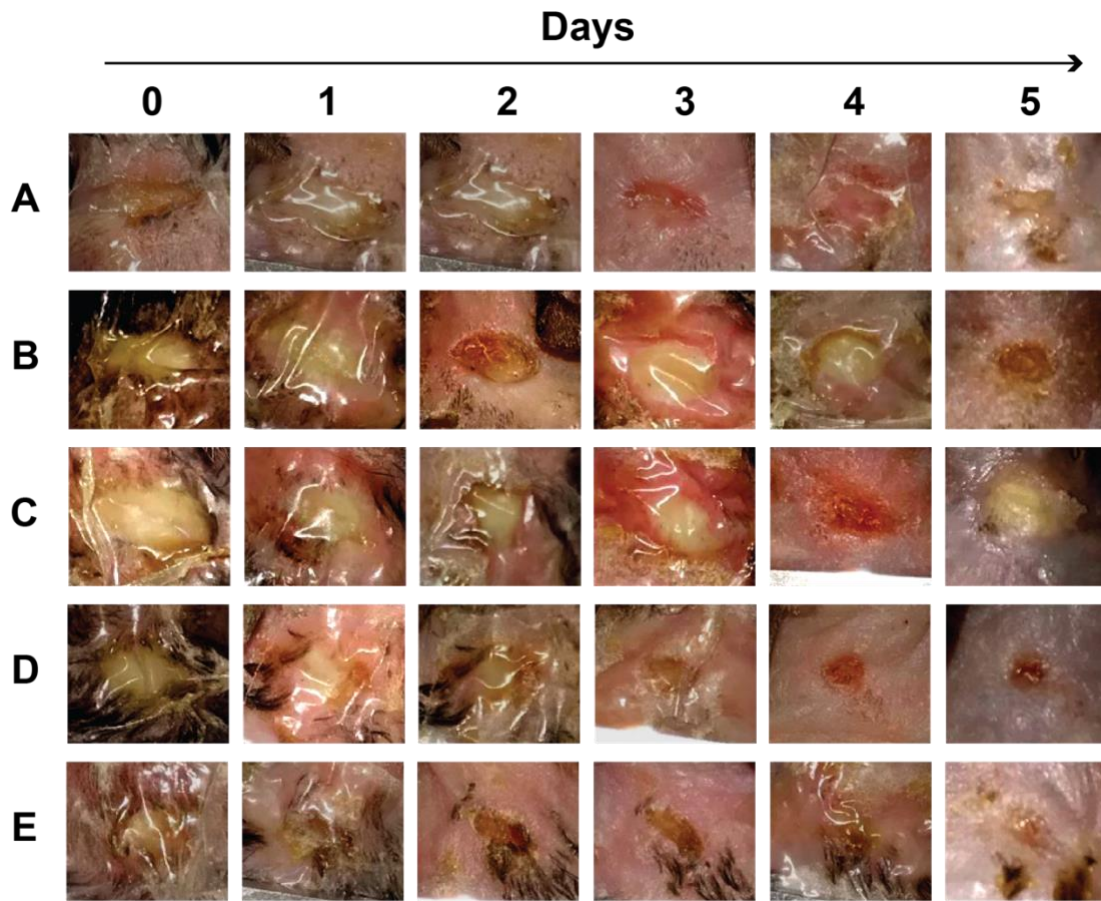
Supplementary Fig S5 | Purulence scoring system. We used a 6-scale system, from 0 to 5, to evaluate the degree of pus formation in wound beds. Scores of 5 indicate that the wound is heavily infected, with pus extending beyond the wound edge. Scores of 4 indicate that the infected wound has significant pus formation but is limited to the wound bed. Scores of 3 are given to wounds completely covered with whitish exudate. Scores of 2 are assigned to wounds with a whitish exudate, and a visible wound bed. Scores of 1 are assigned to wounds with a slightly turbid exudate, while scores of 0 indicate a normal appearing wound without any sign of exudate.



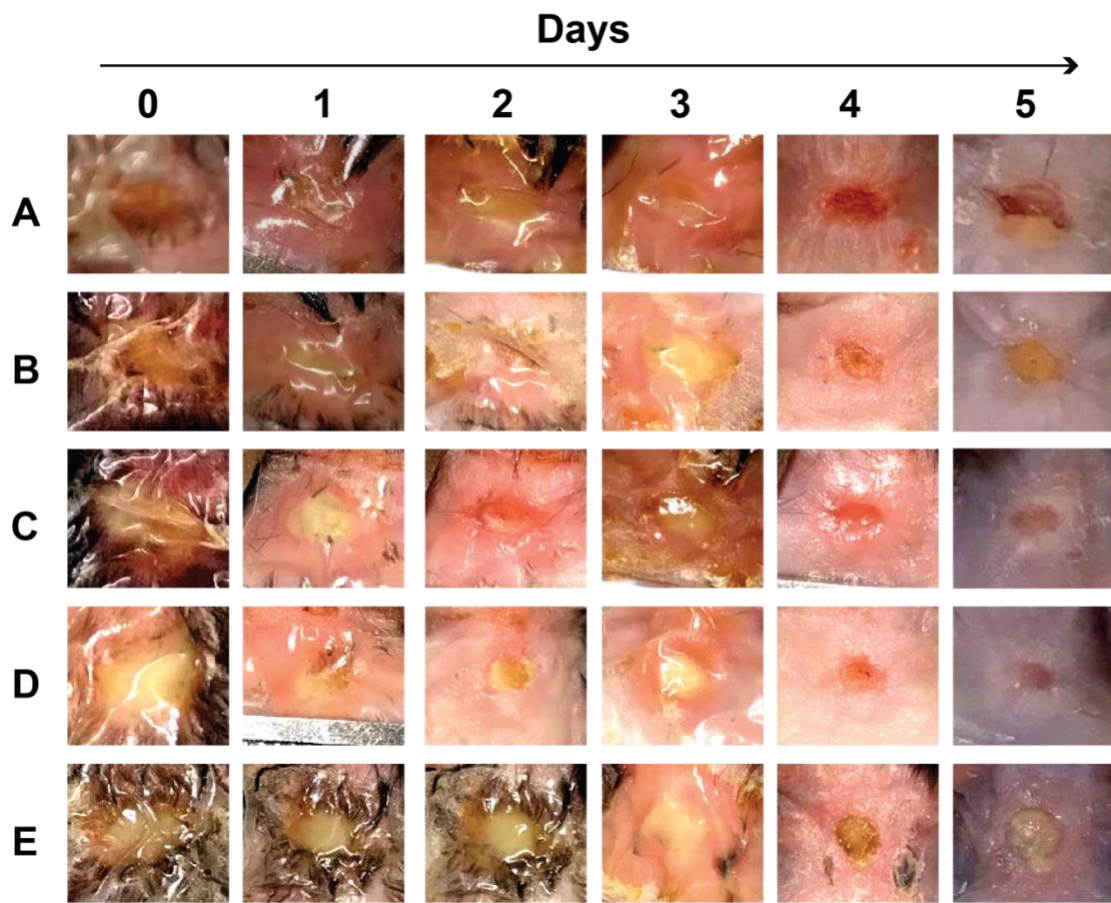
Supplementary Fig S6| Colony counts from the infected wounds treated with PBS and vancomycin. Treatment with vancomycin slightly reduced wound bacterial loads as compared with PBS controls (~ 0.5 log₁₀ unit reduction) after administration of two treatments (* = P values < 0.05).



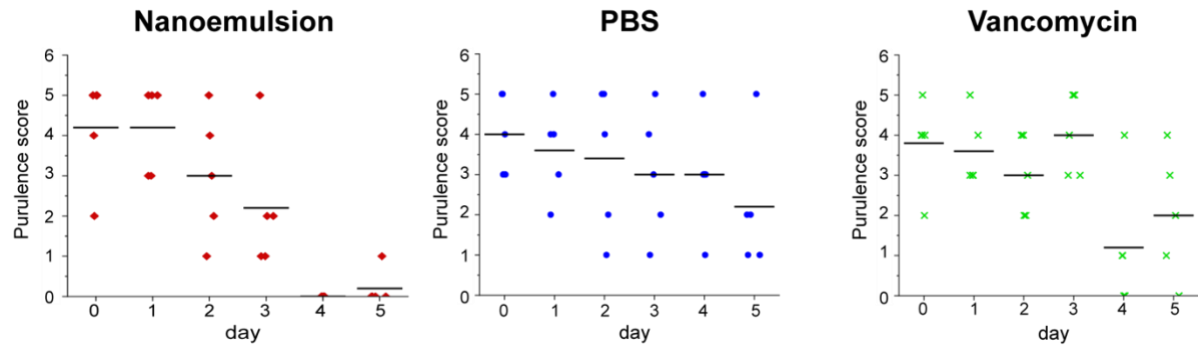
Supplementary Fig S7 | Photographs of infected wounds treated with gelatin nanoemulsions. Photographs were taken daily over the duration of the experiment. Images were used for the blinded evaluation of degrees of purulence.



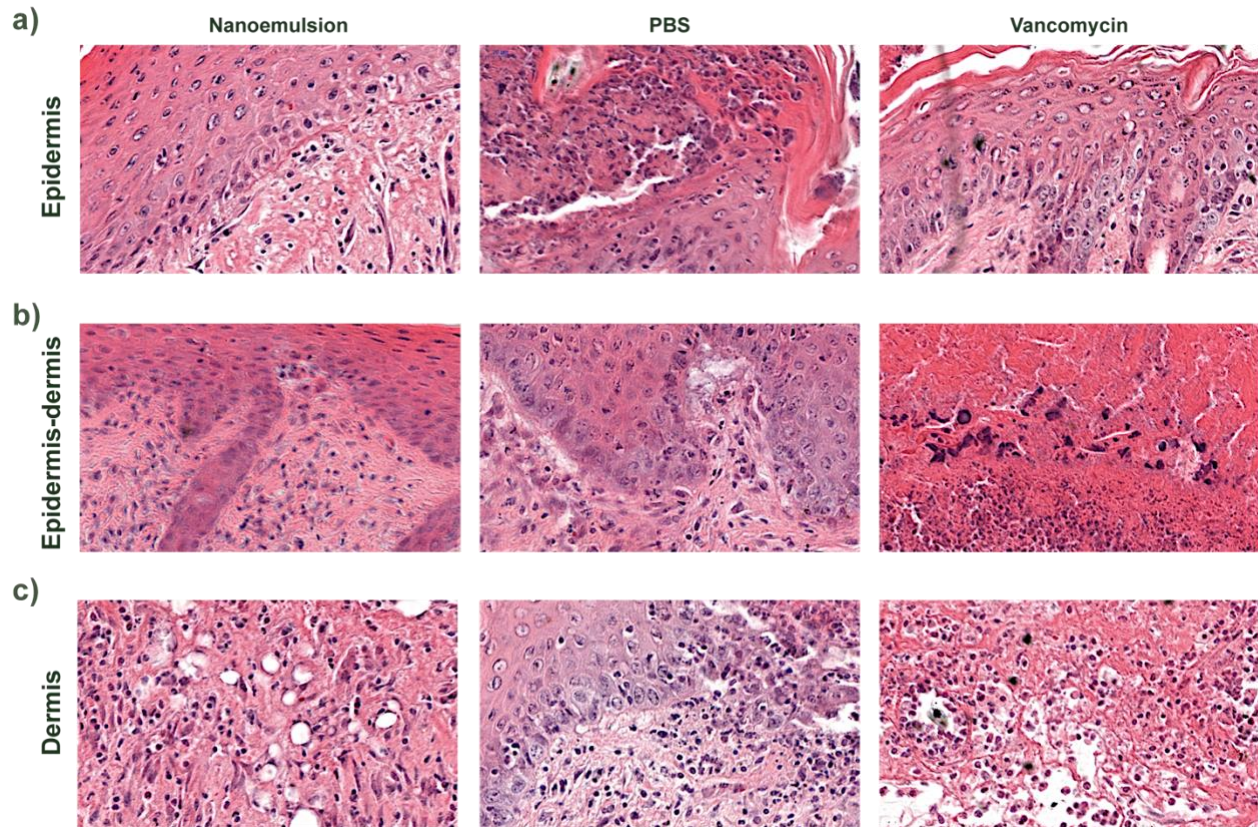
Supplementary Fig S8 | Photographs of infected wounds treated with PBS. Photographs were taken daily over the duration of the experiment. Images were used for the blinded evaluation of degrees of purulence.



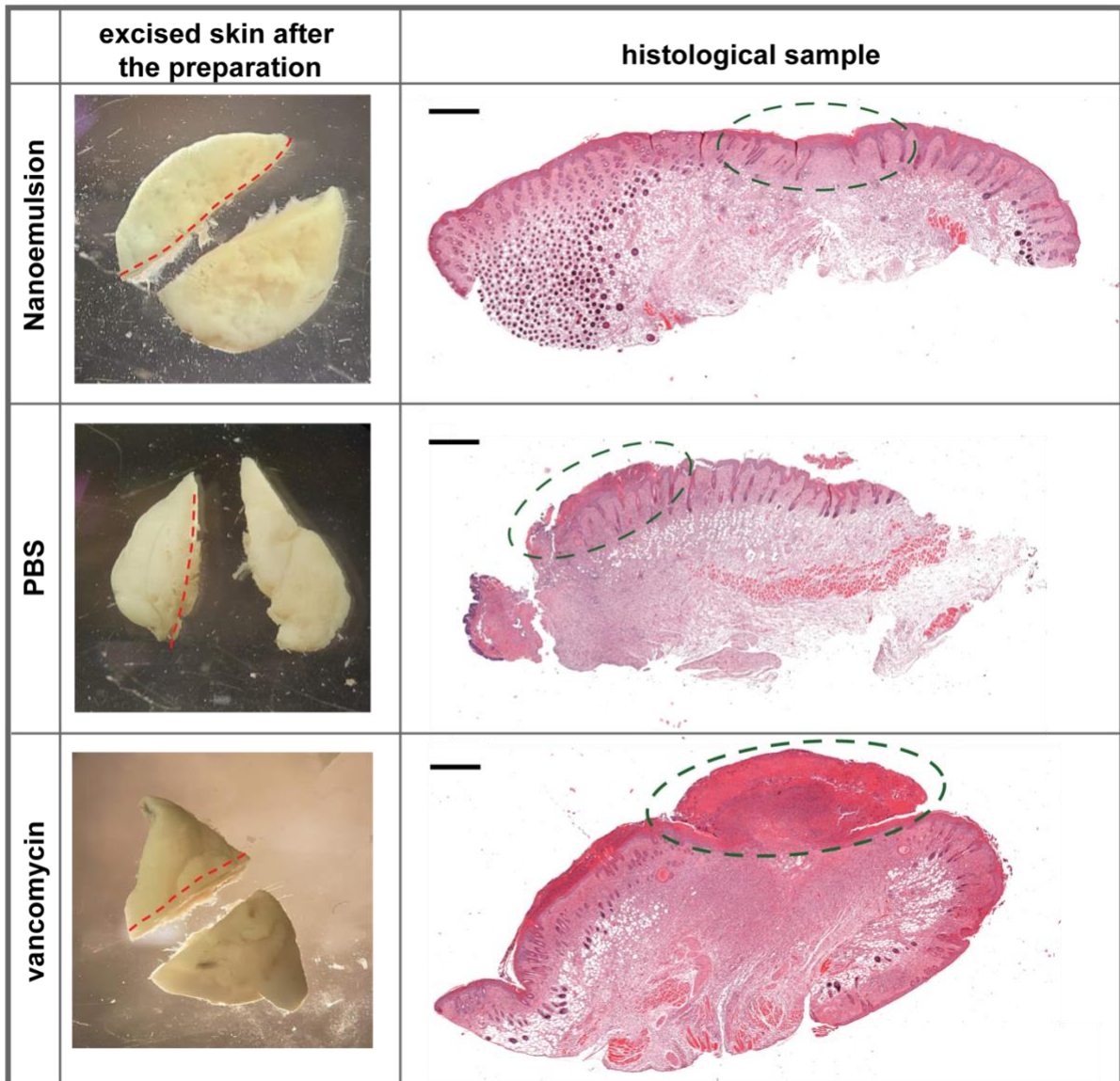
Supplementary Fig S9 | Photographs of infected wounds treated with vancomycin. Photographs were taken daily over the duration of the experiment. Images were used for blinded evaluation of degrees of purulence.



Supplementary Fig S10| Purulence scores of wounds treated with nanoemulsions, PBS, and vancomycin. Photos of infected wounds were taken daily and were used to rate the extent of pus in a blinded fashion. The results showed that treatment with gelatin nanoemulsions resulted in better wound healing than treatment with vancomycin or PBS.



Supplementary Fig S11 | Additional histological samples of skin surrounding infected wounds. a, Epidermis samples showing regeneration of keratin and epithelial layer with nanoemulsion treatment. Inflammatory cells and proteinaceous debris were observed with PBS and vancomycin treatments. **b,** Formation of collagen matrix in epidermis-dermis junction after nanoemulsion treatment. Immature epidermis and granulation were observed with PBS. Necrosis and cell debris were detected in the vancomycin-treated sample. **c,** The dermis was restored with nanoemulsion treatment, while inflammatory cells were still present in other controls.



Supplementary Fig S12 | Excised skin after histological sample preparation – macroscopic and microscopic images. The red dashed line indicates where the histological sample was taken. The green dashed circles indicate the location of wound infection. Scale bar is 500 μm .

Supplementary Table S2 | Information of bacterial strains from Cooley Dickinson Hospital provided by Dr. Riley

	Riley Strain Name	CD-2	CD-1412	CD-1006	CD-489
	Species	<i>Escherichia coli</i>	<i>Enterobacter cloacae</i> complex	<i>Pseudomonas aeruginosa</i>	<i>Staphylococcus aureus</i> - methicillin-resistant
	Date Isolated	9/11/2011	7/12/2006	4/23/2012	3/12/2001
	CFU/mL	>100,000	>100,000	>100,000	>100,000
	Note		Urine from nephrostomy tube		
Aminoglycosides	Amikacin		S		
	Gentamicin	S	I	S	S
	Kanamycin High Level				
	Tobramycin		R		
Penicillin	Ampicillin	R		S	
	Ampicillin/ Sulbactam	I		S	R
	Amoxicillin/ Clavulanate				R
	Oxacillin				R
	Penicillin				R
Cephalosporin	Cefaclor				R
	Ceftriaxone	S	S	S	R
	Cefotaxime				R
	Cefazolin	S	R	S	
	Ceftizoxime				
	Cefepime	S	S	S	

	Cefoxitin	S	R	S	
	Cefuroxime				R
Carbapenem	Imipenem			S	R
Macrolide	Azithromycin				
	Erythromycin				
Fluoroquinolone	Ciprofloxacin	S	S	S	
	Levofloxacin	S	S	S	R
	Ofloxacin				
Lincosamide	Clindamycin				
Oxazolidinone	Linezolid		S		S
Rifamycin	Rifampin				S
Folate pathway inhibitor	Trimethoprim/ Sulfamethoxazole	S	R	S	S
Tetracycline	Tetracycline				S
Glycylcycline	Tigecycline				
Glycopeptide	Vancomycin				S

Supplementary Table S3 | Information of bacterial strains from Mayo Clinic

Strain Name	IDRL-6169	IDRL-10366	IDRL-11442	IDRL-11999
Species	<i>Staphylococcus aureus</i>	<i>Escherichia coli</i>	<i>Pseudomonas aeruginosa</i>	<i>Klebsiella pneumoniae</i>
Date Isolated	8/2000	--	11/5/2014	--
Specimen	Hip tissue	--	Groin isolate	--
Susceptibilities (in µg/mL)	Daptomycin 0.25 S Linezolid 3 S Levofloxacin ≥32 R Minocycline 0.25 S Trimethoprim/sulfamethoxazole 0.094 S Rifampin 0.008 S Vancomycin 0.38 S Ceftaroline 0.5 S Ciprofloxacin >128 R Tedizolid 0.5 S	Imipenem/Relebactam 0.5 S* Ceftolozane/Tazobactam 64 R Imipenem 8 R Meropenem 4 R Ertapenem 16 R Ceftriaxone >128 R Cefepime 64 R	Piperacillin/Tazobactam >64/4 R Cefepime >16 R Ceftazidime >16 R Meropenem >8 R Aztreonam >16 R Ciprofloxacin >2 R Levofloxacin >4 R Amikacin ≤8 S Gentamicin ≤1 S Tobramycin ≤1 S Colistin ≤2 S	Amikacin 32 I Amoxicillin/Clavulanate >16 I Ampicillin >16 I Aztreonam >8 I Cefazolin >4 I Cefotaxime 64 R Cefoxitin >16 I Ceftaroline >2 R Ceftazidime >128 R Ceftriaxone >32 R Chloramphenicol 16 I Ciprofloxacin >2 R Colistin >4 R Doripenem >4 R Ertapenem >4 R Gentamicin ≤4 S Imipenem >4 R Levofloxacin >4 R Meropenem >8 R Piperacillin >64 I

				Piperacillin/Tazobactam >64 I Tigecycline 1 ** Tobramycin >8 R Trimethoprim/sulfamethoxazole >2 R
--	--	--	--	--

*Based on FDA breakpoints; **No breakpoints available in the Clinical Laboratory Standards Institute guidelines.

Reference

- ¹ R. K. Pettit, C. A. Weber and G. R. Pettit, *Ann. Clin. Microbiol. Antimicrob.*, 2009, **8**, 28.
- ² B. Duncan, X. Li, R. F. Landis, S. T. Kim, A. Gupta, L. S. Wang, R. Ramanathan, R. Tang, J. A. Boerth and V. M. Rotello, *ACS Nano*, 2015, **9**, 7775–7782.
- ³ M. Werthén, H. LINA, P. Ø. Jensen, C. Sternberg, M. M. Givskov and T. Bjarnsholt, *APMIS*, 2010, **118**, 156–164.
- ⁴ H. Ceri, M. E. Olson, C. Stremick, R. R. Read, D. Morck and A. Buret, *J. Clin. Microbiol.*, 1999, **37**, 1771–1776.
- ⁵ J. J. Harrison, C. A. Stremick, R. J. Turner, N. D. Allan, M. E. Olson and H. Ceri, *Nat. Protoc.*, 2010, **5**, 1236–1254.
- ⁶ C. K. Kim, M. J. Karau, K. E. Greenwood-Quaintance, A. Y. Tilahun, A. Krogman, C. S. David, B. S. Pritt, R. Patel and G. Rajagopalan, *Toxins (Basel)*, 2015, **7**, 5308–5319.
- ⁷ V. Au and S. A. Madison, *Arch. Biochem. Biophys.*, 2000, **384**, 133–142.
- ⁸ A. S. McCall, S. Kraft, H. F. Edelhauser, G. W. Kidder, R. R. Lundquist, H. E. Bradshaw, Z. Dedeic, M. J. C. Dionne, E. M. Clement and G. W. Conrad, *Invest. Ophthalmol. Vis. Sci.*, 2010, **51**, 129–138.